Wideband Power Combining of Four Microfabricated W-Band Traveling-Wave Tubes

Wang, Shaomeng; Aditya, Sheel

2017

Wang, S., & Aditya, S. (2017). Wideband Power Combining of Four Microfabricated W-Band Traveling-Wave Tubes. IEEE Transactions on Electron Devices, 64(9), 3849-3856.

https://hdl.handle.net/10356/88097

https://doi.org/10.1109/TED.2017.2720191

Wideband Power Combining of Four Microfabricated W-band Traveling-Wave Tubes

Shaomeng Wang, *Member, IEEE* and Sheel Aditya, *Senior Member, IEEE*

***Abstract*— Wideband power combining of four W-band microfabricated traveling-wave tubes (TWTs) is presented. The proposed TWTs are based on a planar helix slow-wave structure (SWS) with straight-edge connections (PH-SEC) that can be microfabricated with stripline input/output feed. A novel 1:4 WR-10 waveguide-to-stripline power divider/combiner is designed that covers the frequency range of 92 GHz-104 GHz. The simulation results show that S_{11} is less than –20 dB and the magnitude and phase differences among the four output signals are less than 0.01 dB and 0.41°, respectively, indicating a power combining efficiency as high as 99.9%. The power divider, four PH-SEC SWSs, and the power combiner are assembled and the performance of the overall assembly is checked by simulation. The overall S_{11} is better than –15 dB in the frequency range of 91.7 GHz-100.7 GHz and S_{21} is better than –12.3 dB. Effects of power and phase variation of individual TWTs have also been considered. With four 5 kV and 10 mA sheet electron beams, particle-in-cell (PIC) simulations show that the combined TWTs can give 25 W saturation peak power at 94 GHz with a gain of 18 dB.**

***Index Terms*— Power combining, wideband, microfabrication, sheet beam, traveling-wave tube**

I. Introduction

MICROWAVE and millimeter wave frequencies have very important applications in modern society [1]. In particular, the W-band frequency range (75–110 GHz) is useful for communications, radar, spectroscopy etc. [2]. In these applications, it is very desirable to get a power amplifier with high power, gain and wide bandwidth. Among these properties wide bandwidth enables higher rate of information transmission and a better resolution of radar imaging. The W-band frequency range can provide sufficiently wide bandwidth for such applications.

One of the important features of travelling-wave tubes (TWTs) is operation over a wide bandwidth with high gain. As a consequence, there has been strong interest in developing W-band TWTs with high power in the recent years. At such high frequencies, the physical dimensions of the various parts of TWTs become quite small [3], making it very challenging to achieve the required accuracy using traditional fabrication processes. To address this problem, various slow-wave structures (SWSs) that can be microfabricated have been proposed in the recent years [4]-[7] An SWS is a very important part of a TWT. But TWTs incorporating a microfabricated SWS generally offer modest output power levels.

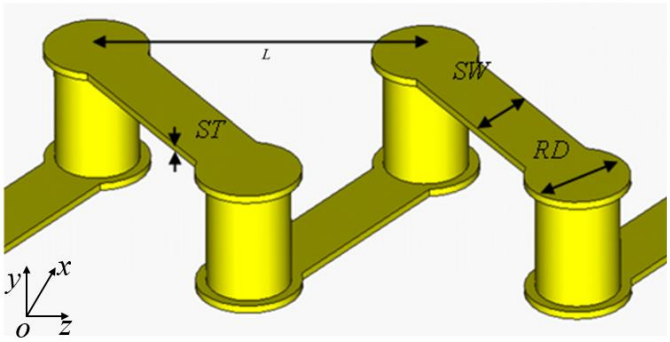

Fig.1. Planar helix SWS with straight-edge connections (PH-SEC) [8].

The recently proposed planar helix with straight-edge connections (PH-SEC), shown in Fig. 1, is readily amenable to microfabrication [8]. It has been demonstrated that this structure retains the broadband property of the circular helix. Besides, its aspect ratio can be changed to accommodate a sheet beam which can offer advantages such as higher beam current capacity, decreased beam voltage, lower magnetic field requirement and increased bandwidth [9].

Especially keeping in view the feasibility of microfabrication, a wideband configuration of the PH-SEC for operation at W-band has also been proposed recently [10]. Fig. 2 shows the cross-section of this configuration which achieves a wide bandwidth and can accommodate a sheet beam. The PIC simulation results show that the small-signal gain of such a W-band PH-SEC TWT can reach 36.8 dB and the 3-dB bandwidth is about 60%. But the output power at 3.7 W is quite modest.

One approach to increase the output power of such a TWT is to employ power combining. There are many schemes that have been reported for power combining for both solid state electronics devices [11]-[13] and vacuum electronics devices [14]-[18]. These schemes include binary Wilkinson power combiners, T-junction waveguide power combiners and quasi-optical power combiners [19]-[22]. The binary Wilkinson

Manuscript received April, 2017. This work was partially supported by a grant from the Office of Space Technology and Industry (OSTIn), Singapore.

S. Wang and S. Aditya are with the School of Electrical and Electronic Engineering, Nanyang Technological University, Singapore 639798 (e-mail: wangsm@ntu.edu.sg; esaditya@ntu.edu.sg).

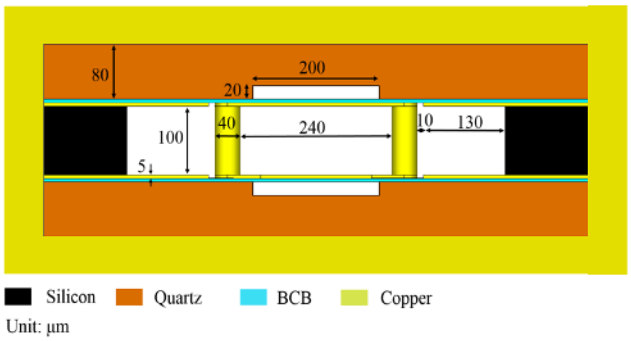

Fig. 2. Cross-section of the W-band PH-SEC SWS together with dimensions.

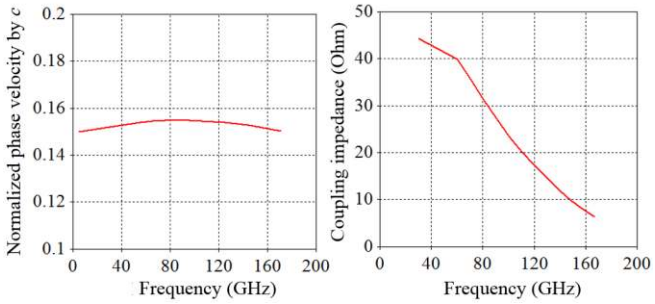

Fig. 3 (a) Dispersion and (b) coupling impedance characteristics of the W-band PH-SEC SWS.

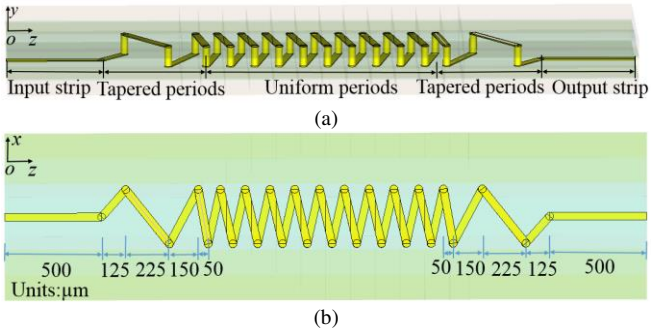

Fig. 4 Structures of the PH-SEC SWS with 10 periods and input and output stripline feeds. The metal enclosure is not shown. (a) 3-D view, and (b) 2-D view with main dimensions.

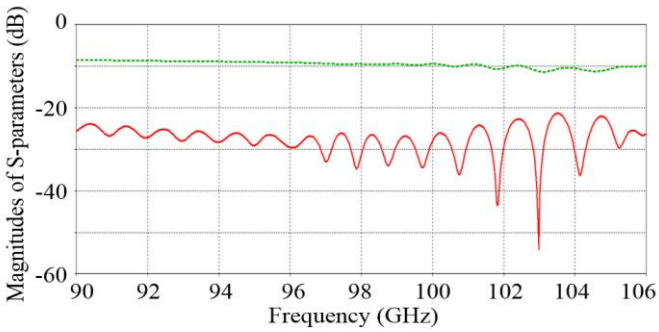

Fig. 5 S-parameters of the PH-SEC SWS with 200 periods and input and output stripline feeds.

power combiner is widely used for solid state devices. The waveguide power combiner is used when the required output power is relatively high. The quasi-optical power combiners are adopted to combine power for a rather large number of devices [23].

In this paper, our goal is to combine the output power of four PH-SEC TWTs that are driven by four independent electron beams, using waveguide input/output ports. For this purpose, we propose a combination of 1:2 WR10 waveguide-to-waveguide power divider/combiner and a 1:2 WR10 waveguide-to-stripline power divider/combiner to achieve 4-way power combining. Compared to the binary Wilkinson power combiner, the power combiner proposed here is more suitable for vacuum electronic devices. Compared to a 1:4 waveguide power combiner, the overall size of the proposed combiner is much smaller. The structure of the proposed combiner is also much simpler than that for the quasi-optical power combiner schemes. The waveguide-to-stripline power divider can provide a power combining efficiency as high as 99.9%. Moreover, the waveguide-to-waveguide power divider/combiner can be cascaded to form a $1:2^n$ power combiner to produce a much higher combined power.

The paper is organized as follows. Section II describes the W-band PH-SEC SWS structure and its dispersion and coupling impedance. Section III presents the design of the stripline feed for the PH-SEC SWS. In section IV, the 1:4 waveguide-to-stripline power divider/combiner is realized in two steps: the first step involves a 1:2 waveguide-to-stripline power divider/combiner; then a 1:2 waveguide-to-waveguide power divider/combiner is implemented by using the magic T junction. Section V describes the PIC results of the combined PH-SEC TWTs. Section VI discusses the effect of power and phase variation of individual TWTs on the power combining efficiency. Section VII concludes the paper.

II. W-BAND PH-SEC SWS

Fig. 2 shows the W-band PH-SEC SWS used in this paper. This is a modification of the SWS in [10] and uses a metal enclosure instead of vertical metal pillar arrays and horizontal metal layers for shielding. Getting rid of the shielding pillars and shielding metal layers of [10] simplifies the fabrication process considerably. All simulation results include the metal enclosure but the rest of the figures showing this SWS omit the metal enclosure for the sake of clarity.

The properties of the materials in the SWS are set as below: dielectric constant and loss tangent of quartz are 4.43 and 5.1×10^{-5}, respectively; conductivity of copper for our fabrication is estimated to be 2×10^7 S/m; dielectric constant and loss tangent of silicon are 11.9 and 2.5×10^{-4}, respectively; dielectric constant of BCB (Cyclotene) is 2.65 [24].

Fig. 3(a) shows the phase velocity vs. frequency for the proposed structure using the dimensions given in Fig. 2 and a period of 128 μm. Simulations have been carried out using CST Microwave Studio [25]. Similar to [10], the phase velocity shows only a small variation over a large frequency range. The dispersion curve is different from a normal helical SWS in which phase velocity falls with increasing frequency. Such a behaviour (including negative dispersion) is seen when the metal shield comes rather close to the SWS and there are also CPW ground planes [26]. The coupling impedance shown in Fig. 3 (b) has a relatively high value of about 23.6 Ohms at 100 GHz.

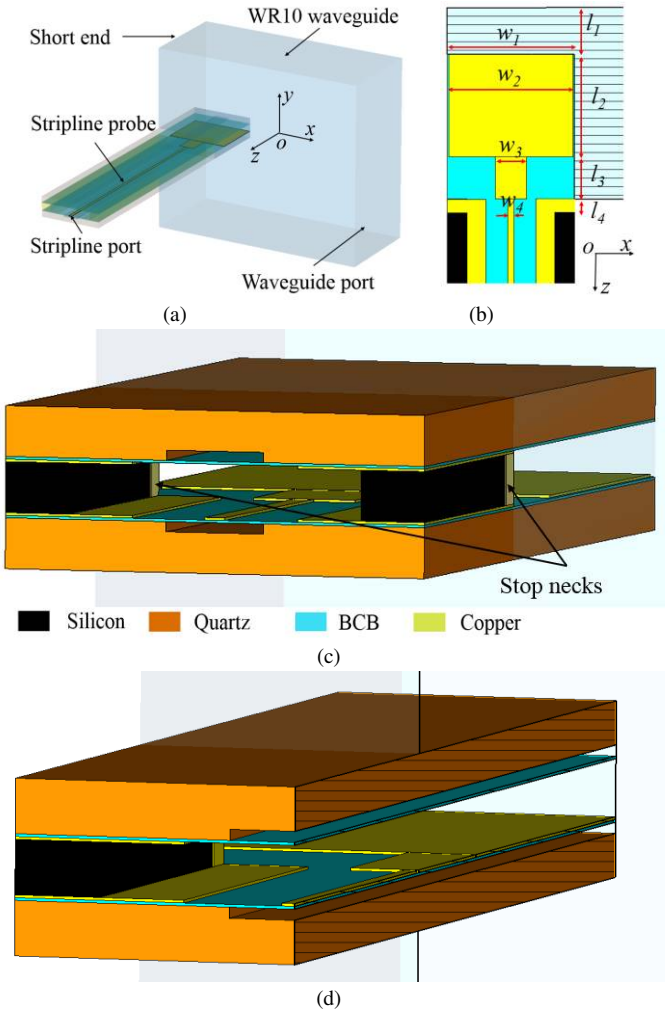

Fig. 6 W-band waveguide-to-stripline adaptor. (a) 3-D view, (b) dimensions and (c) details of the stripline probe, (d) cut-away view of the probe.

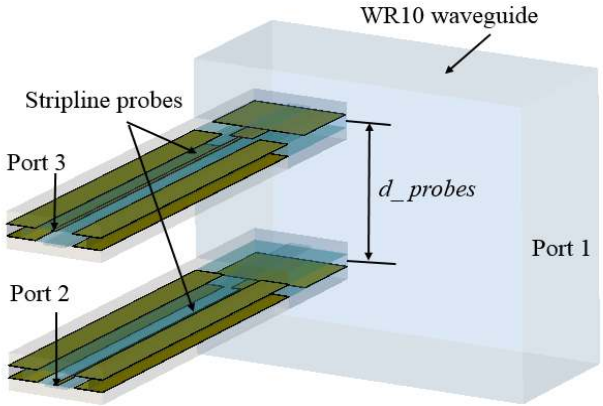

Fig. 7 Perspective view of the 1:2 waveguide-to-stripline power divider.

The flat dispersion characteristics of the proposed structure enable relatively wideband impedance matching and beam-wave interaction.

III. Stripline Feed For W-band PH-SEC Slow-wave Structure

As shown in Fig. 1, the PH-SEC SWS consists of vertical pillars connected by horizontal strips. As a result, it is convenient to use stripline as input/output feed lines connecting to the horizontal strips. Also, a waveguide-to- stripline power divider/combiner can be more compact than a waveguide-to-waveguide power divider/combiner.

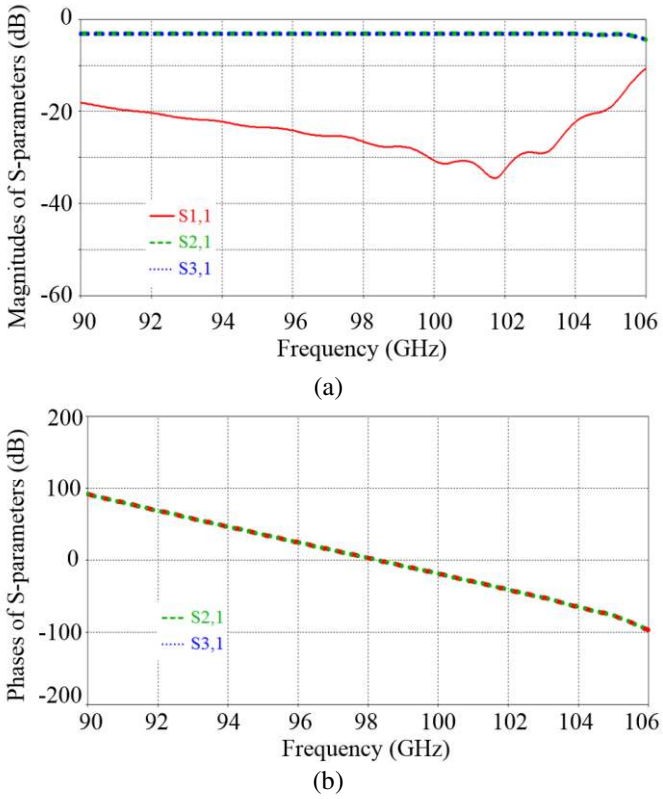

Fig. 8 S-parameters of the 1:2 waveguide-to-stripline power divider. (a) Magnitudes of S_{11}, S_{21}, S_{31} and (b) phases of S_{21} and S_{31}.

Fig. 4 (a) shows the PH-SEC SWS with 10 periods and stripline input/output feeds which consist of approximately two tapered periods of PH-SEC and a section of stripline at both ends to get a good match. The stripline feeds are in the same layer as the horizontal strips of the PH-SEC; thus both features can be fabricated in the same process step. Fig. 4 (b) shows the top view of the PH-SEC structure with stripline feeds; this figure also includes the taper dimensions.

Fig. 5 shows the S-parameters of the stripline feeds applied to a 200-period PH-SWS structure. S_{11} is better than –20 dB while S_{21} is around –10 dB in the frequency range of 83 GHz-108 GHz, indicating a bandwidth of 26% centered at 95.5 GHz.

IV. Waveguide-To-Stripline Power Divider

To handle the combined output power of four PH-SEC TWTs, we need a waveguide output port. Hence, to keep the overall structure symmetric, we use a waveguide port at the input also. To implement a 1:4 power divider/combiner with waveguide input/output ports, we propose a combination of 1:2 waveguide-to-waveguide power divider/combiner and a 1:2 waveguide-to-stripline power divider/combiner. Compared to a 1:4 waveguide power combiner, the overall size of the proposed combiner is much smaller. The design procedure of the 1:4 rectangular waveguide-to-stripline power divider is described in the following.

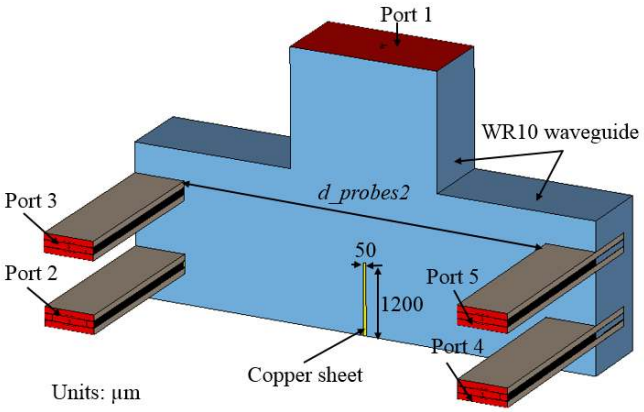

Fig. 9 Perspective view of the 1:4 waveguide-to-stripline power divider.

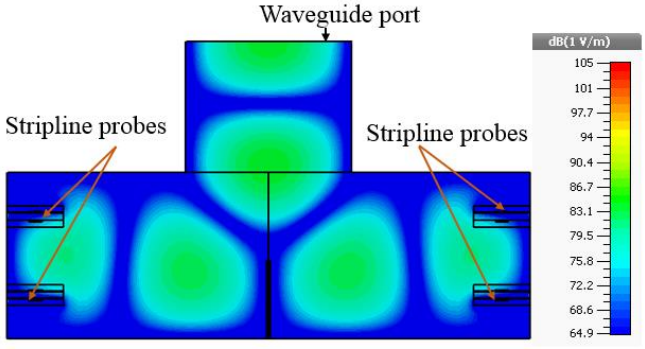

Fig. 10 Magnitude pattern of the electric field inside the 1:4 waveguide-to-stripline power divider.

A. *Stripline-to-rectangular waveguide adaptor*

For implementing a 1:2 waveguide-to-stripline power divider/combiner, a stripline-to-waveguide adaptor is required. The proposed adaptor, shown in Figs. 6, involves extending the stripline feed described in the previous section and inserting it into the WR-10 rectangular waveguide to act as a probe to excite the TE_{10} mode. The probe is inserted through the middle of the broad wall of the rectangular waveguide. With reference to Figs. 2 and 6(a), there is shielding above and below the stripline due to the metal enclosure. But the stripline probe inside the waveguide does not have such shielding; of course the probe 'sees' the top and bottom waveguide walls.

The stripline probe consists of three sections with different widths for wideband impedance matching. One stop-neck is located at each end of the silicon support to guarantee good alignment between the probe and the waveguide. The main dimensions of the stripline probe are marked in Fig. 6 (b). The structure details of the stripline probe are shown in Figs. 6 (c) and (d); as can be seen the probe has the same substrate structure as the PH-SEC SWS shown in Fig. 2.

The effects of the fabrication tolerances on the performance of the stripline-to-waveguide adaptor have been studied. The simulation results show that for a variation of ±10 µm in the dimensions marked in Fig. 6(b), the changes in the S-parameters are quite small. The effect of misalignment between the stripline probe and the waveguide has also been studied. With reference to Fig. 6(a), for misalignments along the *x, y* and *z* directions of 30 µm, 50 µm, and 50 µm respectively, the insertion loss does not change by more than 0.2 dB and the −20 dB S_{11} bandwidth remains unchanged. But there is a 2-3% shift in the center frequency of operation.

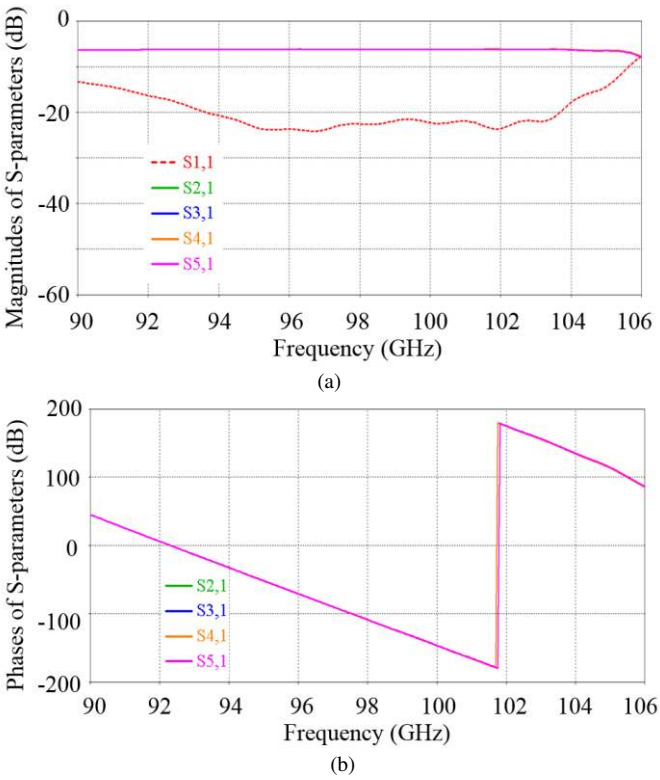

Fig. 11 S-parameters of the 1:4 waveguide-to-stripline power divider; (a) magnitude, and (b) phase.

B. *1:2 waveguide-to-stripline power divider*

Next, based on the stripline-to-waveguide adaptor, the 1:2 waveguide-to-stripline power divider is designed. As shown in Fig. 7, the two stripline probes are arranged symmetrically about the mid-plane of the broad wall of the waveguide so that two identical signals can be obtained from Ports 2 and 3 when Port 1 is set as the input port. The distance *d_probes* is the vertical separation between the center-conductors of the stripline probes.

Fig. 8 shows the S-parameters of the 1:2 waveguide-to-stripline power divider using dimensions as *d_probes*=1200 µm, w_1=860 µm, w_2=840 µm, w_3=210 µm, w_4=40 µm, l_1=310 µm, l_2=680 µm, l_3=280 µm, l_4=860 µm. As can be seen, S_{11} is better than –20 dB and S_{21} and S_{31} are equal and close to –3 dB in the frequency range of 92 GHz-105 GHz. Fig. 8(b) shows the phases of S_{21} and S_{31} with no observable difference between the phases. Due to the cosine variation of the TE_{10} E-field in the waveguide, the output drops if a larger vertical separation between the probes is used.

C. *1:4 waveguide-to-stripline power divider*

The just mentioned cosine variation of the E-field also restricts the number of stripline probes that can be 'stacked' vertically in the waveguide. Instead, to realize a 1:4 power

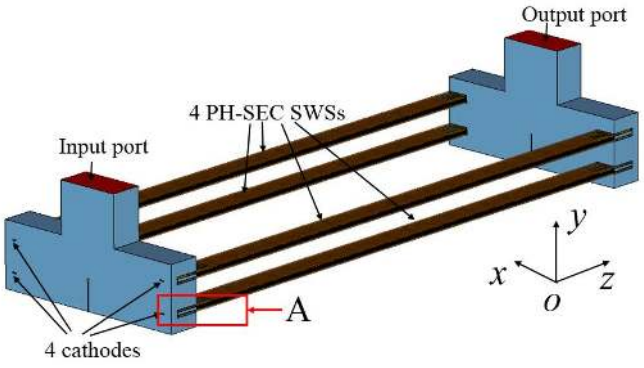

(a)

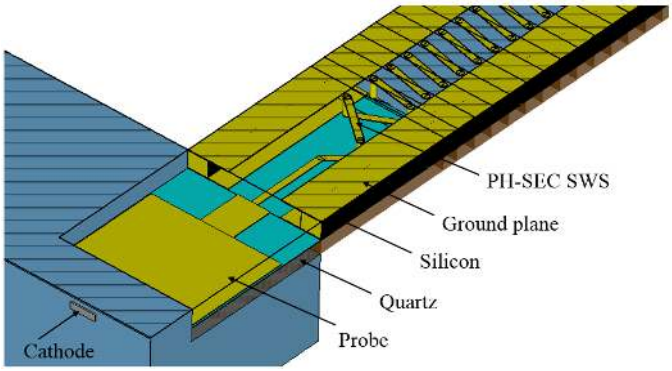

(b)

Fig. 12 (a) Assembled power divider, four PH-SEC SWSs, and power combiner; (b) connection between the probe and SWS.

divider, we cascade a 1:2 waveguide-to-waveguide power divider with the 1:2 waveguide-to-stripline power divider. The rectangular waveguide H-plane T-junction is used as the 1:2 waveguide power divider.

The 1:4 waveguide-to-stripline power divider is shown in Fig. 9. In the center part is the H-plane T-junction, at the bottom of which a thin vertical copper sheet is placed centrally. The width of the copper sheet is the same as the short edge of the rectangular waveguide. By adjusting the thickness and height of the copper sheet, the performance of the power divider can be improved. Each of the two branches of the T-junction is connected to a 1:2 waveguide-to-stripline power divider described before. Ports 2 and 4 are symmetrically located on either side of the copper sheet and so are ports 3 and 5. When a signal is fed to port 1 of the power divider, ideally we expect the signals coming from the four output ports to have the same magnitude and phase. The dimensions are also marked in Fig. 9.

When port 1 is excited, Fig. 10 shows the magnitude pattern of the electric field inside the 1:4 waveguide-to-stripline divider, visually indicating symmetrical power division at the output ports. Since the efficiency of a power divider depends on the differences in the magnitude and phase of the divided signals, Figs. 11(a)-(b) show the magnitudes and phases of the S-parameters of the power divider. Fig. 11(a) shows that S_{11} is better than –20 dB in the frequency range of 94 GHz-104 GHz. The magnitudes of S_{21}, S_{31}, S_{41}, S_{51} appear identical; at 100 GHz these are –6.152 dB, –6.159 dB, –6.152 dB and –6.159 dB, respectively, so that the magnitude difference among the output values is ~0.007 dB. In a similar manner the phases of S_{21}, S_{31},

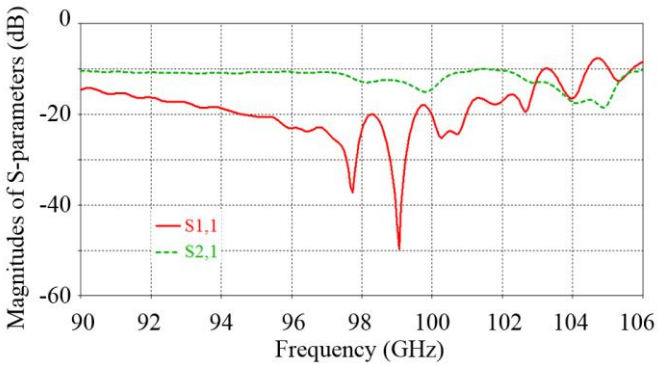

Fig.13 S-parameters of the assembled TWT.

TABLE I.
PARAMETERS OF THE ELECTRON BEAMS

Parameter	Value
Voltage	5.0 kV
Current	10 mA
Beam height	40 μm
Beam width	160 μm
Transmission distance	25.8 mm

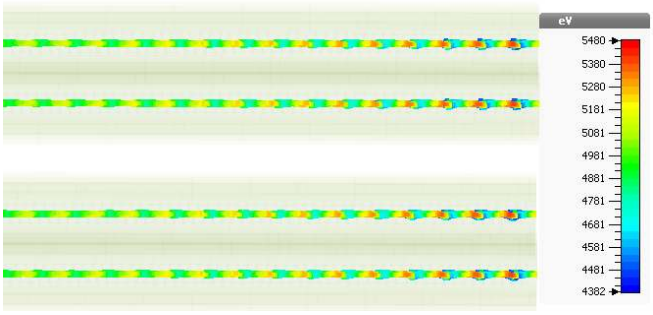

(a)

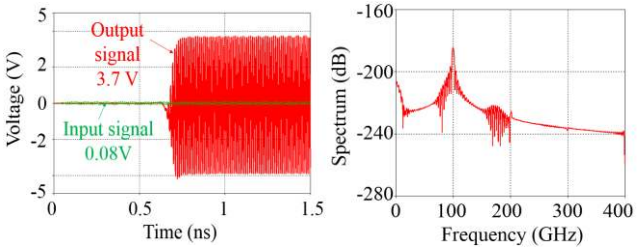

(b) (c)

Fig. 14 Typical PIC results for the overall assembly. (a) Electron beam trajectories near the output end of the SWSs; (b) input and output signals vs. time curves; (c) spectrum of the combined output signal.

S_{41}, S_{51} also appear identical; at 100 GHz these are –146.747°, –146.339°, –146.747° and –146.339°, respectively, so that the maximum phase difference is ~0.41°. According to these phase and magnitude differences, the power combining efficiency can be calculated [14] and it comes to about 99.9% at 100 GHz.

V. POWER OUTPUT OF THE OVERALL ASSEMBLY

To estimate the combined output power of 4 PH-SEC TWTs, we assemble the 1:4 power divider and combiner with four PH-SEC SWSs. Fig. 12 (a) shows the simulation model built in CST for the assembly with common input and output waveguide ports. Fig. 12 (b) shows the details of the connection of the stripline probe and the PH-SEC SWS with tapered periods. The

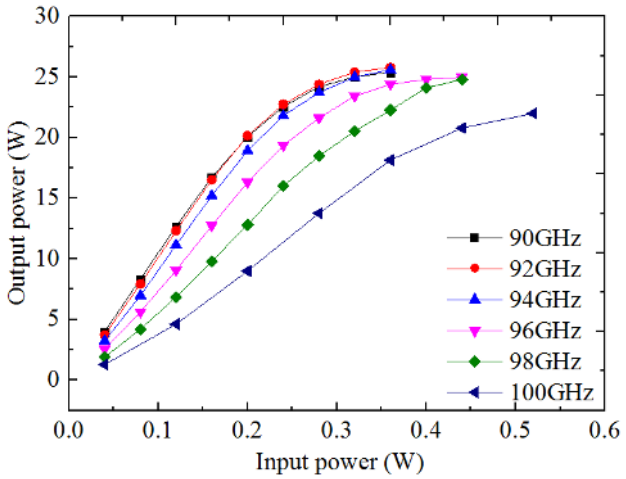

Fig. 15 Output power vs. input power curves at different frequencies with 150-period long SWSs.

transmission properties of the assembly with 200-period long SWSs are shown in Fig. 13; S_{11} is better than –15 dB and S_{21} is better than –12 dB in the frequency range of 92 GHz-102 GHz.

The assembled structure will be placed into an evacuated metal enclosure for shielding and maintaining vacuum. Four electron guns and collectors will be assembled together with the metal enclosure. A single magnetic circuit, similar to the one proposed in [10] can be used to provide the focusing magnetic field for the overall TWT.

To estimate the hot-test performance using particle-in-cell (PIC) simulations, one cathode is defined for each PH-SEC SWS. In practice, the cathodes will be replaced by identical electron guns. A magnetic field of 0.5 T is assumed and the PIC simulations are carried out over the frequency range of 90 GHz-100 GHz. The parameters of the electron beams used in the simulations are listed in Table I.

Fig. 14 presents a typical result obtained from the PIC simulations using CST Particle Studio [26]. Fig. 14 (a) shows the electron beam trajectory and the bunching phenomenon in all four electron beams. Fig. 14 (b) is the magnitude-time curve of the combined output signal at the frequency of 92 GHz. When the input power is set to 8 dBm, the output power can reach 13.69 W, indicating a small signal gain of 33.3 dB. Fig. 14 (c) shows that the spectrum of the output signal is quite clean and does not suffer from oscillations.

But in practice, due to the mismatch between the SWS and input/output ports, the gain of a single section TWT is usually limited to below 26 dB to reduce the risk of oscillation. Thus, in the subsequent results, the length of the SWSs has been reduced to 150 periods.

Fig. 15 shows the output vs. input power curves at different frequencies for the overall assembly. Both the linear and non-linear parts of the curves can be seen. The saturation point occurs at lower input power for lower frequencies. For instance, the saturation input power is 0.36 W for 90 GHz compared to 0.46 W for 98 GHz. This is expected from the coupling impedance vs. frequency curve shown in Fig. 3(b). If we fix the input power at 0.36 W, the output powers are 25.4 W and 18.2 W at 90 GHz and 100 GHz, respectively, indicating a maximum power variation of 1.5 dB in the operating frequency range. If we change the input power to operate the TWT at saturation, the output powers will be 25.4 W and 22 W at 90 GHz and 100 GHz, respectively, indicating a maximum power variation of 0.69 dB. The corresponding saturation gains vary from 18.4 dB to 16.2 dB.

TABLE II.
POWER COMBING EFFICIENCIES FOR DIFFERENT PHASES

Phase 2 (°)	Phase 3 (°)	Phase 4 (°)	Phase 5 (°)	Efficiency (%)
0	0	5	5	99.5
0	0	10	10	99.2
0	0	20	20	95.7
0	20	0	20	96.7
0	0	50	50	77.3
0	50	0	50	79.9
0	5	10	15	97.9
0	10	20	30	94.6
0	20	40	60	82.4

TABLE III.
POWER COMBING EFFICIENCIES FOR DIFFERENT POWERS

Power 2 (W)	Power 3 (W)	Power 4 (W)	Power 5 (W)	Efficiency (%)
1	1	0.81	0.81	99.8
1	1	0.64	0.64	98.7
1	1	0.25	0.25	90.1
1	0.25	1	0.25	88.8
1	0.81	0.64	0.25	94.5

TABLE IV.
POWER COMBING EFFICIENCIES FOR DIFFERENT POWERS AND PHASES

Pow. 2 (W) Pha. 2 (°)	Pow. 3 (W) Pha. 3 (°)	Pow. 4 (W) Pha. 4 (°)	Pow. 5 (W) Pha. 5 (°)	Efficiency (%)
1 0	1 0	0.81 5	0.81 5	90.2
1 0	0.64 20	1 0	0.64 20	78.8
1 0	0.81 5	0.64 10	0.25 15	62.9
1 0	0.81 20	0.64 40	0.25 60	54.3

VI. DISCUSSION

The combining efficiency of 99.9% for the 1:4 rectangular waveguide-to-stripline power divider/combiner in section IV is based on ideal conditions, i.e., the four ports have identical amplitude and phase. Moreover, the four TWTs are very likely to have different output power and phase even for identical input signals. Therefore the effect of power and phase difference on the power combining efficiency should be estimated. Table II lists the power combining efficiency for different phase combinations, assuming that the input power for Ports 2-5 is uniform at 1 W. When the phase differences are less than 10°, the power combining efficiency can be higher than 99%. When the phase differences are 50°, the power combining efficiency can drop to 77.3%.

Table III lists the power combining efficiency for different power combinations, assuming that the input phase for Ports 2-5 is identical. As can be seen, when the power difference is less

than 2 dB, the power combining efficiency is higher than 98.7%. When the power difference reaches 6 dB, the power combining efficiency can reduce to 88.8%.

Table IV lists the power combining efficiency for different power and phase combinations. When the power difference is less than 1 dB together with the phase difference less than 5 degrees, the power combining efficiency can be higher than 90%. In the rather extreme case when the power difference reaches 6 dB and the phase difference reaches 60 degrees, the power combining efficiency can reduce to 54.3%.

VII. Conclusion

This paper has described the power combining of four W-band TWTs that employ four microfabricated planar-helix SWSs and four sheet electron beams. To realize 1:4 power combining with waveguide input/output ports, a novel 1:4 rectangular waveguide-to-stripline power divider/combiner has been designed with a high combining efficiency of 99.9% in the ideal case. The assembled TWT, including the power divider, four PH-SEC SWSs and the power combiner, shows a reflection coefficient better than –15 dB and an insertion loss better than –12.3 dB in the frequency range of 91.7 GHz-100.7 GHz. When the assembly is excited with four 5.0 kV and 10 mA sheet electron beams, the combined TWT has been predicted to produce 25 W saturation output power with a gain of 18 dB at 94 GHz. The power combining efficiency has also been estimated for the likely case in which the four TWTs do not have identical output power and phase and is seen to drop depending upon the extent of difference.

References

[1] R. J. Barker, N. C. Luhmann, J. H. Booske, and G. S. Nusinovich, 'Modern microwave and millimeter-wave power electronics', *IEEE Press*, USA, 2005.

[2] R. H. Abrams, B. Levush, A. A. Mondelli, and R. K. Parker, "Vacuum electronics for the 21st century," *IEEE Microwave Magazine*, pp: 61-72, Sep. 2001.

[3] A. S. Gilmour, Jr., "Principle of Traveling Wave Tubes," *Artech House*, INC., 1994.

[4] S. Sengele, H. Jiang, J. H. Booske, C. L. Kory, D. W. van der Weide, and R. L. Ives, "Microfabrication and Characterization of a Selectively Metallized W-Band Meander-Line TWT Circuit" *Electron Devices, IEEE Transactions on*, vol. 56(5), pp: 730-737, May 2009.

[5] M. R. Lueck, D. M. Malta, K. H. Gilchrist, C. L. Cory, G. T. Mearini, and J. A. Dayton, "Microfabrication of diamond-based slow-wave circuits for mm-wave and THz vacuum electronic sources," *Journal of Micromechanics and Microengineering*, 21 (2011) 065022 (7pp), May 2011.

[6] C. Chua, J. M. Tsai, S. Aditya, M. Tang, S. W. Ho, Z. Shen, and L. Wang , "Microfabrication and Characterization of W-Band Planar Helix Slow-Wave Structure with Straight-Edge Connections," *Electron Devices, IEEE Transactions on*, vol. 58(11), pp. 4098-4105, 2011.

[7] C. L. Kory, J. A. Dayton, G. T. Mearini, D. Malta, M. Lueck, K. Gilchrist, and B. Vancil, "95 GHz helical TWT design," *Proc. IEEE Int. Vac. Electron. Conf.*, Rome, 28–30 April, 2009, pp: 125-126.

[8] C. Chua, S. Aditya, and Z. Shen, "Planar helix with straight-edge connections in the presence of multilayer dielectric substrates," *Electron Devices, IEEE Trans. on*, vol. 57, no. 12, pp: 3451-3459, Dec. 2010.

[9] C. Zhao, S. Aditya, S. Wang, and C. Chua, "A wideband planar helix slow-wave structure for millimeter-wave TWTs", *Vacuum Electronics Conference (IVEC), 2015 IEEE International*, S15.5, Beijing, Apr. 2015.

[10] S. Wang, S. Aditya, J. Miao, and X. Xia, "Design of a sheet-beam electron-optical system for a microfabricated W-band traveling-wave tube using a cold cathode", *Electron Devices, IEEE Transactions on*, vol. 63(9), pp: 3725-3732, Jul. 2016.

[11] X. Jiang, S. C. Ortiz, and A. Mortazawi, "A Ka-band power amplifier based on the traveling-wave power-dividing/combining slotted-waveguide circuit," *Microwave Theory and Techniques, IEEE Transactions on*, vol. 52(2), pp: 633-639, Feb. 2004.

[12] L. W. Epp, D. J. Hoppe, A. R. Khan, and S. L. Stride, "A high-power Ka-band (31–36GHz) solid-state amplifier based on low-loss corporate waveguide combining", *Microwave Theory and Techniques, IEEE Transactions on,* vol. 56(8), pp: 1899-1908, Aug. 2008.

[13] J. Jeong, Y. Kwon, S. Lee, C. Cheon, and E. A. Sovero, "1.6- and 3.3-W power-amplifier modules at 24 GHz using waveguide-based power-combining structures," *Microwave Theory and Techniques, IEEE Transactions on*, vol. 48(12), pp: 2700-2708 Dec. 2000.

[14] J. Ge, Y. Zhou, B. Yu, C. Zhu, J. Zhou, J. Li, F. Wan, J. Feng, J. Cai, and X. Wu, "Pulsed power combining system for W-band traveling wave tube amplifiers with a waveguide combiner," *Electron Devices, IEEE Transactions on*, vol. 61(9), pp: 3317-3323, Sep. 2014.

[15] A. Elfrgani, H. Seidfaraji, S. C. Yurt, M. I. Fuks, and E. Schamiloglu, "Power combiner for high power cerenkov devices," *IEEE International Vacuum Electronics Conference*, 2008, Monterey, CA, pp: 183-184, Apr. 2008.

[16] R. N. Simons, E. G. Wintucky, J. D. Wilson, and Dale A. Force, "Ultra-high power and efficiency space traveling-wave tube amplifier power combiner with reduced size and mass for NASA missions," *Microwave Theory and Techniques, IEEE Transactions on,* vol. 57(3), pp: 582-588, Mar. 2009.

[17] R. Xiao, Y. Deng, Y. Wang, Z. Song, J. Li, J. Sun, and C. Chen, "Power combiner with high power capacity and high combination efficiency for two phase-locked relativistic backward wave oscillators", *Applied Physics Letters*, vol. 107, pp: 133502-1-4, Sep. 2015.

[18] A. Srivastava, "Particle-in-cell simulation for W-band power combiner multibeam planar coupled-cavity backward wave oscillator", *European Journal of Advances in Engineering and Technology*, vol. 2(10), pp: 66-69, 2015.

[19] X. Shan, and Z. Shen, "An eight-way power combiner based on a transition between rectangular waveguide and multiple microstrip lines, " *Microwave Theory and Techniques, IEEE Transactions on*, vol. 61(7), pp: 2585-2593 Jul. 2013.

[20] K. Song, Y. Fan and Y. Zhang. "A microstrip probe coaxial waveguide power divider/combiner," *Int J Infrared Milli Waves*, vol. 27, pp: 1269-1279, Jul. 2006.

[21] R. J. Hwu, C. F. Jou, N. C. Luhmann, JR., M. Kim, W. W. Lam, Z. B. Popovic, and D. B. Rutledge, "Array concepts for solid-state and vacuum microelectronics millimeter-wave generation," *Electron Devices, IEEE Transaction on*, vol. 36(11), pp: 2645-2650, Nov. 1989.

[22] R. J. Hwu, J. Ren, D. K. Kress, S. V. Judd, J. M. Krebs, L. P. Sadwick, A. T. Burke, and J. J. Petillo, "Ku band, 100 kW traveling wave tube based on large quasi-optical spatial power combining array," *IEEE International Vacuum Electronics Conference*, 2016, Monterey, CA, pp: 1-2, Apr. 2016.

[23] M. P. DeLisio and R. A. York, "Quasi-optical and spatial power combining," *Microwave Theory and Techniques, IEEE Transactions on*, vol. 50(3), pp: 929-936, Mar. 2002.

[24] *Property of Cyclotene Advanced Electronics Resins*, accessed on 10 Jan. 2017. [Online]. Available: http://www.dow.com/cyclotene/

[25] *Introduction of CST Microwave Studio*, accessed on 1 Dec. 2016. [Online] https://www.cst.com/products/cstmws

[26] K. Swaminathan, C. Zhao, C. Chua, and S. Aditya, "Vane-Loaded Planar Helix Slow-Wave Structure for Application in Broadband Travelling-Wave Tubes," *Electron Devices, IEEE Transaction on*, vol. 62(3), pp: 1017-1023, Mar. 2015.

[27] *Introduction of CST Particle Studio*, accessed on 1 Dec. 2016. [Online] https://www.cst.com/products/cstps

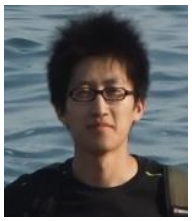

Shaomeng Wang (M'15) received the Ph.D. degree from the University of Electronic Science and Technology of China, Chengdu, China in 2013.

He is currently Research Fellow with Nanyang Technological University, Singapore. He is also with the Southwest Jiaotong University, Chengdu, China. His current interests are mainly focused on the vacuum electron devices.

Sheel Aditya (S'76–M'80–SM'94) received the B.Tech. and Ph.D. degrees in electrical engineering from IIT Delhi, Delhi, India, in 1974 and 1979, respectively.

He has been an Associate Professor with the School of Electrical and Electronic Engineering, Nanyang Technological University, Singapore, since 2001. His current research interests include microfabricated vacuum electron devices.